Oxygen reduction reaction on La$_{0.8}$Sr$_{0.2}$Co$_x$Fe$_{1-x}$O$_{3-\delta}$ perovskite/carbon black electrocatalysts in alkaline medium

Alexandros Safakas, Georgios Bampos, Symeon Bebelis*

Department of Chemical Engineering, University of Patras, Caratheodory 1, University Campus, GR-26504, Patras, Greece

ABSTRACT

A series of La$_{0.8}$Sr$_{0.2}$Co$_x$Fe$_{1-x}$O$_{3-\delta}$ (LSCF) perovskite oxides, including La$_{0.8}$Sr$_{0.2}$CoO$_{3-\delta}$ (LSC) and La$_{0.8}$Sr$_{0.2}$FeO$_{3-\delta}$ (LSF), were synthesized via a combustion method and, mixed with carbon black at a mass ratio 3:1, were studied towards their oxygen reduction reaction (ORR) activity in 0.1 M KOH solution at room temperature, using the thin-film rotating disk electrode (RDE) technique. The highest and lowest ORR (specific and mass) activities among the tested electrocatalysts were exhibited by LSC and LSF, respectively. Increasing Co content and at the same time decreasing Fe content in the LSCF composition, resulted in ORR specific activity enhancement as well as in an increase in the number of transferred electrons, from ca. 2 (for LSF) to ca. 4 (for LSC), implying a change in the ORR mechanism. The observed change in ORR activity of the perovskite/C electrocatalysts upon gradual substitution of iron by cobalt was associated with induced changes in the surface B-sites electronic structure and in surface oxygen vacancy formation.

1. Introduction

Market expansion of proton exchange membrane fuel cells (PEMFCs) and anion exchange membrane fuel cells (AEMFCs) is rather limited due mostly to the sluggish kinetics of oxygen reduction reaction (ORR) and the related use of high cost Pt-based electrocatalysts [1–5]. Aiming to overcome these barriers and achieve acceptable ORR efficiency at the lowest possible cost, various research groups have focused on study and development of novel non-precious metal electrocatalysts for ORR [5–9].

Faster ORR kinetics, which in principle allows for the use of non-noble metal electrocatalysts, and less corrosive environment, in which a wider range of electrocatalysts are stable, are major advantages of alkaline media over acidic media [5], justifying the recent increased research interest towards AEMFCs [2,3]. Non-noble metal electrocatalysts which have been studied as ORR electrocatalysts in alkaline media include mainly carbon-transition metal hybrids, nonmetal-doped nanocarbons and transition metal oxides [5,9]. Among the latter are Co-based oxides [10], spinels [11,12] and perovskites [8,13].

The oxygen reduction to OH$^-$ in alkaline media is described by the overall reaction:

$$O_2 + 2H_2O + 4e^- \rightarrow 4OH^- \tag{1}$$

Alternatively, O$_2$ can be reduced to HO_2^-, according to the reaction:

$$O_2 + H_2O + 2e^- \rightarrow HO_2^- + OH^- \tag{2}$$

The peroxide ion can be further reduced to OH$^-$:

$$HO_2^- + H_2O + 2e^- \rightarrow 3OH^- \tag{3}$$

or subjected to disproportionation:

$$2HO_2^- \rightarrow O_2 + 2OH^- \tag{4}$$

Reaction (1) corresponds to the so called direct or 4e$^-$ pathway, reaction (2) to the 2e$^-$ pathway, whereas reactions (2) & (3) to the (serial) 2e$^-$ + 2e$^-$ pathway. The term "pseudo 4e$^-$ pathway" is also typically used where differentiation between the direct 4e$^-$ and the 2e$^-$ + 2e$^-$ pathways is not possible. The ORR pathway and rate determining steps depend on the electrocatalyst [5,14], whereas the mechanistic aspects of ORR in alkaline medium and the factors governing the ORR activity have not been completely clarified despite the progress towards this direction [5,8,10–13].

Considering their low cost and the ability to fine-tune their catalytic properties via tailoring their composition, ABO$_3$ type perovskite oxides, where A is a lanthanide and B a transition metal, as well as their partially substituted counterparts AA'BB'O$_3$, where A' is an alkaline earth and B' another transition metal, have attracted significant interest as potential ORR electrocatalysts for application in alkaline environment [5,8,13,15–17]. Although the overall reaction is the same, the ORR mechanism on these perovskites is different than that on precious

---

* Corresponding author.
  E-mail addresses: simeon@chemeng.upatras.gr, S.Bebelis@upatras.gr (S. Bebelis).

metals [5,14]. The catalytic cycle of ORR to OH^- (Eq. (1)) consists of four steps with participation of one electron at each step [5,8]. In the first step, H_2O interacts with surface lattice oxygen ($B^{(m+1)+}$- O^{2-}) at the B (or/and B′) sites to generate surface hydroxide groups ($B^{m+} - OH^-$) which, in the next step, are displaced by oxygen (exchanged with adsorbed O_2^-, resulting from $O_2 + e^- \rightarrow O_2^-$) yielding to formation of peroxide ions ($B^{(m+1)+}$- O_2^{2-}). Then, the peroxide ions interact with H_2O to produce OH^- and oxyhydroxide groups ($B^{m+} - OOH^-$). The final step in the catalytic cycle is the regeneration of the surface oxide groups via removal of OH^-. The rate determining step is either the O_2^-/OH^- exchange step (formation of surface peroxide ions) or the surface hydroxide generation step, depending primarily on whether there is more or less than one e_g electron at the surface B (or/and B′) cation, respectively [8]. It has also been demonstrated by Suntivich et al. [8] that ORR activity on perovskite oxides primarily correlates to e_g orbital filling of the surface B-site cations and, secondarily, to the covalency of the B-site transition metal–oxygen bond, although other electronic structure factors of the transition metal sites have also been reported to affect ORR activity [13,17,18]. In the case of $2e^-$ pathway (Eq. (2)), the catalytic cycle consists of two steps; the displacement of surface hydroxide groups ($B^{m+} - OH^-$) by adsorbed O_2^- to form surface peroxide species ($B^{(m+1)+}$- O_2^{2-}), as described above, and the interaction of the latter with H_2O to form HO_2^- and regenerate surface hydroxide.

Reports on the use of ABO_3-type perovskites as ORR electrocatalysts appeared in literature already since mid-1970s, when Matsumoto et al. [19] studied $LaNiO_3$ as catalyst for cathodic reaction of oxygen. Recently, Suntivich et al. [20] reported an ORR specific activity of $LaNiO_3$/C equal to 1/8 of that of Pt/C (40 $\mu A\ cm_{oxide}^{-2}$ vs. 320 $\mu A\ cm_{Pt}^{-2}$) at 0.9 V vs. RHE in 0.1 M KOH, pointing out the significant potential for development of active perovskite-based ORR electrocatalysts. $LaMnO_3$/C was found by Hyodo et al. [21] to exhibit the highest ORR activity, in 8 M KOH, among a series of $LnMnO_3$/C perovskites, where Ln: Pr, Nd, Sm, Gd, Y, Dy, Yb, La. Stoerzinger et al. [22] studied the ORR activity of epitaxially oriented $La_{1-x}Sr_xMnO_3$ in 0.1 M KOH as a function of Sr substitution; they reported that $La_{0.67}Sr_{0.33}MnO_3$, containing mixed $Mn^{3+/4+}$ was the most active for ORR and pointed out the important role of mixed Mn valence and fast charge transfer at the oxide/H_2O interface in obtaining high ORR activity. Xue et al. [23] reported that the oxygen adsorption capacity and ORR activity of Sr-doped lanthanum manganites, in 0.1 M KOH, can be optimized by properly adjusting Sr doping and introducing A-site deficiency; $(La_{0.7}Sr_{0.3})_{0.98}MnO_3$/C exhibited the highest ORR activity among $(La_{1-x}Sr_x)_{0.98}MnO_3$/C (x = 0.2 - 0.5) and $La_{0.7}Sr_{0.3}MnO_3$/C electrocatalysts. Sunarso et al. [24] compared the ORR activity of $LaMO_3$/C and $LaNi_{0.5}M_{0.5}O_3$/C (M = Ni, Co, Fe, Mn and Cr) electrocatalysts in 0.1 M KOH. They found that $LaCoO_3$/C and $LaNi_{0.5}Mn_{0.5}O_3$/C were the most active among the tested $LaMO_3$/C and $LaNi_{0.5}M_{0.5}O_3$/C electrocatalysts, respectively. Poux et al. [25] compared the ORR mechanism on $LaCoO_3$/C and $La_{0.8}Sr_{0.2}MnO_3$/C in 1 M NaOH; they concluded that it follows predominately a series pathway with formation of HO_2^- as intermediate, in particular for low oxide loadings and in the absence of carbon in the electrocatalytic layer. Moreover, they reported a higher ORR activity for $La_{0.8}Sr_{0.2}MnO_3$/C and a lower HO_2^- yield. A high activity for ORR in 0.1 M KOH and a predominant $4e^-$ pathway was reported by Jin et al. [26] for $Ba_{0.5}Sr_{0.5}Co_{0.8}Fe_{0.2}O_3$/C, which was also an excellent electrocatalyst for oxygen evolution reaction (OER) [27]. Very recently, Alegre et al. [28] studied $La_{0.6}Sr_{0.4}Co_{0.2}Fe_{0.8}O_3$/C as a bifunctional ORR/OER electrocatalyst in 1 M KOH. They reported that $La_{0.6}Sr_{0.4}Co_{0.2}Fe_{0.8}O_3$/C was less active than Pd/C, which was used as benchmark electrocatalyst, the onset potential for $La_{0.6}Sr_{0.4}Co_{0.2}Fe_{0.8}O_3$/C being shifted by ca. 0.1 V to more cathodic values; on the contrary, it was found significantly more active than Pd/C as it concerns OER.

In the present work a series of $La_{0.8}Sr_{0.2}Co_xFe_{1-x}O_3$ (LSCF) perovskite oxides, including $La_{0.8}Sr_{0.2}CoO_3$ (LSC) and $La_{0.8}Sr_{0.2}FeO_3$ (LSF), were synthesized via a combustion method and, mixed with carbon black (Vulcan XC-72R), studied towards their oxygen reduction reaction activity in O_2-saturated 0.1 M KOH solution at room temperature, using the thin-film rotating disk electrode (RDE) technique. To the best of our knowledge, it is the first time that the effect of gradual substitution of iron by cobalt in the B-sites of $La_ySr_{1-y}Co_xFe_{1-x}O_3$ perovskites is systematically studied as it concerns ORR electrocatalytic activity and ORR mechanism in alkaline media.

2. Experimental

2.1. Synthesis of perovskite powders

The perovskite powders were synthesized using the combustion synthesis method, starting from nitrate precursors [29–31]. La$(NO_3)_3$·$6H_2O$ (Alfa Aesar, 99.9% REO), $Sr(NO_3)_2$ (Sigma-Aldrich, 99 + % ACS), $Co(NO_3)_2$·H_2O (Sigma-Aldrich, ≥ 99% KT) and $Fe(NO_3)_3$·$9H_2O$ (Merck, ≥ 99%) were used as precursors, whereas citric acid monohydrate (Merck, 99.5 – 100.5 % assay) was used as propellant (fuel).

Proper amounts of metal nitrates were dissolved in triple distilled water at room temperature. The resulting solution was mixed with a (ca. 1.7 M) citric acid solution (mole ratio of citric acid to metal ions equal to 2:1), adding also an amount of NH_4NO_3 (Merck, ≥ 99%) as extra-oxidant (mole ratio of NH_4NO_3 to metal ions equal to 1:1) [30]. Addition of NH_4NO_3 is expected to improve the specific surface area of the perovskite via decreasing the reaction time, as it has been reported for the combustion synthesis of $LaMnO_3$ [30]. Finally, ammonia solution (30 wt. %, Carlo Erba) was added dropwise to reach a pH value of ca. 9. This step is needed for neutralization of the citric acid excess [32] and enhancement of the stabilization of the metal citrates species in the resulting colloidal solution (sol) [33]. The final solution was heated on a hot plate at 200 °C. After evaporation of H_2O, the mixture was heated to 400 °C using a heat gun. Within seconds after reaching 400 °C, the mixture started to foam and, finally, ignited forming a thin crust, which was then easily shattered into a thin powder. The powder was heated to 900 °C with a ramp rate of 5 °C min^{-1} and was calcined at this temperature for 5 h, under stagnant air, in order to develop the perovskite phase. After cooling, the powder was finely ground via pestling in an agate mortar for approximately half an hour.

Six $La_{0.8}Sr_{0.2}Co_xFe_{1-x}O_{3-\delta}$ perovskite oxides, with x = 0, 0.2, 0.4, 0.6, 0.8 and 1, were prepared and tested. The short-names used to refer to them in the present work are listed in Table 1.

2.2. Physicochemical characterization

The specific surface areas (SSA) of the synthesized perovskite powders were determined via the BET method in a Micromeritics TriStar 3000 apparatus, employing nitrogen physical adsorption at liquid N_2 temperature, after previous degassing of the powders under vacuum at 300 °C for 1 h.

X-ray diffraction (XRD) was used for phase characterization of the perovskite powders. The XRD data were collected at room temperature over the 2θ range 10 – 90° and at a scan rate equal to 0.04° s^{-1}, using a Bruker AXS D8 Advance diffractometer, equipped with a Cu-Kα lamp

Table 1

Composition and specific surface area (SSA) of the synthesized perovskite oxides.

Perovskite	Notation	SSA (m² g⁻¹)
$La_{0.8}Sr_{0.2}FeO_{3-\delta}$	LSF	7.2
$La_{0.8}Sr_{0.2}Co_{0.2}Fe_{0.8}O_{3-\delta}$	LSCF_8228	5.6
$La_{0.8}Sr_{0.2}Co_{0.4}Fe_{0.6}O_{3-\delta}$	LSCF_8246	4.7
$La_{0.8}Sr_{0.2}Co_{0.6}Fe_{0.4}O_{3-\delta}$	LSCF_8264	6.8
$La_{0.8}Sr_{0.2}Co_{0.8}Fe_{0.2}O_{3-\delta}$	LSCF_8282	5.5
$La_{0.8}Sr_{0.2}CoO_{3-\delta}$	LSC	5.7

(λ = 1.54062 Å) and a Ni filter. Phase analysis and identification was made via the EVA software (Bruker AXS).

The exact stoichiometry of the synthesized powders was determined by Inductively Coupled Plasma Optical Emission Spectroscopy (ICP-OES) using a Perkin Elmer Optima 7000 DV ICP-OES system. No significant differences were found between the nominal and the determined stoichiometry.

2.3. Electrodes preparation and electrochemical characterization

The electrocatalytic activity for ORR of the prepared perovskites was evaluated via the rotating disk electrode (RDE) technique, in O_2 saturated 0.1 M KOH solution and at room temperature (ca. 20 °C). A glassy-carbon (GC) disk electrode of 5 mm diameter (0.196 cm^2 geometric surface area) was used (RDE.GC50, Metrohm Autolab B.V.), which was mounted on a RDE holder (RDE-2 Metrohm Autolab B.V.). Each tested perovskite oxide, mixed with carbon black (Vulcan XC-72R, Cabot), was deposited on the glassy carbon RDE in the form of a thin film, as described below, and was used as the working electrode in a typical three-electrode system, where the electrolyte was 0.1 M KOH aqueous solution contained in a Teflon vessel. A Pt foil (0.8 cm x 0.5 cm) electrode and a Ag/AgCl (3 M KCl) electrode (Metrohm A.G.) were used as counter and reference electrode, respectively. The potential of the Ag/AgCl electrode was measured equal to 0.960 V vs. RHE in H_2 saturated 0.1 M KOH and ca. 20 °C. To prepare the electrocatalysts, the synthesized perovskite oxides were mechanically mixed with a high surface area carbon black (Vulcan XC-72R, specific surface area 216 m^2 g^{-1}) to facilitate electrical contact between oxide particles in the tested electrodes, thus favoring complete utilization of the perovskite surface [34]. The perovskite-carbon mixture was pulverized in a mortar, using the appropriate amount of each material in order to obtain a perovskite to carbon mass ratio equal to 3:1 [35]. The resulted powder was deposited on the polished glassy carbon RDE surface using a suspension of the powder in a mixture of 2-propanol (Merck, ACS Reag.) and triple distilled water. After homogenizing the suspension via ultasonication, it was dropwise added onto the GC electrode using a pipette and subsequently dried at room temperature. A suspension containing 5% wt. Nafion solution (Sigma Aldrich), 2-propanol (Merck, ACS Reag.) and triple distilled water was then added onto the dried film, to act as a binding agent [36], and was left to evaporate at room temperature. Additional details concerning the electrocatalyst deposition procedure can be found elsewhere [37]. A perovskite loading of the working electrode equal to 74 μg_{oxide} cm_{disk}^{-2} was used, determined by increasing the loading up to a value beyond which no change in the calculated (from Koutecky –Levich plots) limiting current density was observed. A loading independent limiting current density has been used as a criterion for reliable experimental results in thin-film RDE studies employing carbon supported metal electrocatalysts [36].

ORR activity characterization involved recording of polarization curves in O_2 saturated 0.1 M KOH solution via scanning linearly the potential of the electrocatalyst from -0.6 to 0.1 V vs. Ag/AgCl (0.36 to 1.06 V vs. RHE) at a scan rate of 5 mV s^{-1}, for five different rotation rates (830, 1250, 1750, 2350 and 3000 rpm) of the RDE. An Autolab PGSTAT302 N galvanostat/potentiostat controlled by the NOVA software (Metrohm Autolab) was used for this purpose. The electrolyte resistance, as determined via electrochemical impedance spectroscopy, was equal to ca. 45 Ω. No ohmic drop correction was applied. From the analysis of the ORR polarization curves, employing Koutecky-Levich (K-L) plots, the kinetic current and electron transfer number were calculated and compared for all tested electrocatalysts, as described below. Prior to ORR activity characterization, the potential of each tested electrocatalyst was continuously cycled in the above range in He saturated 0.1 M KOH solution, until a stable reproducible cyclic voltammogram was recorded.
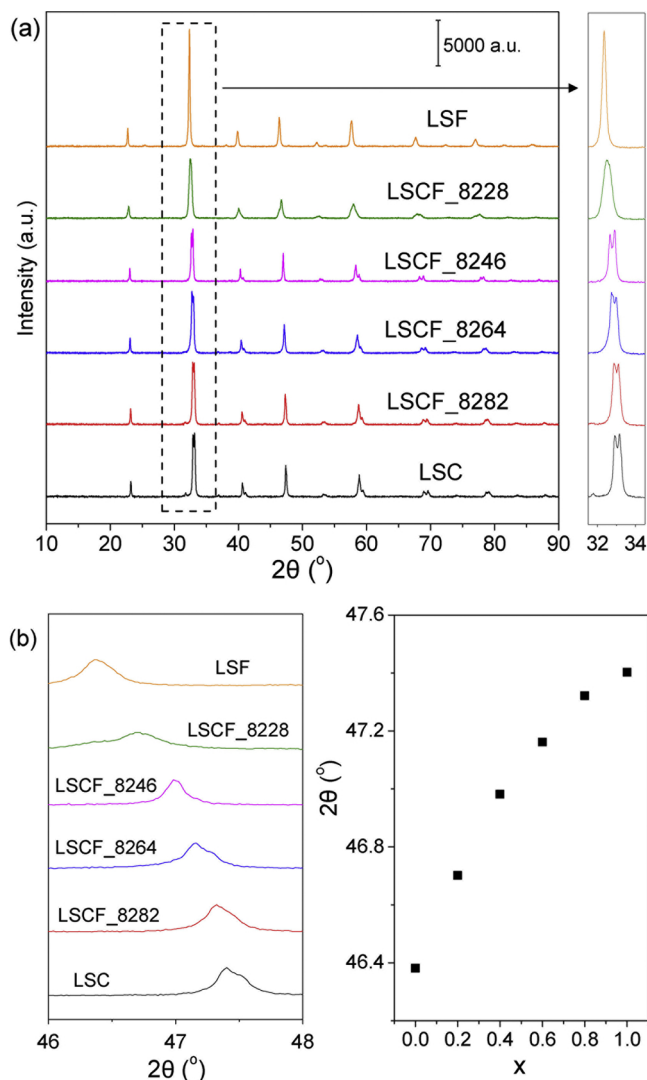

Fig. 1. (a) X-ray diffraction (XRD) patterns of the prepared $La_{0.8}Sr_{0.2}Co_xFe_{1-x}O_{3-\delta}$ perovskite powders (Table 1). (b) Detail of the XRD patterns in the 2θ range 46 to 48° (left) and dependence of the position of the XRD peak in this range on Co/(Fe + Co) molar ratio x (right).

3. Results and discussion

The measured specific surface areas (SSA) of the synthesized perovskite powders varied from 4.7 m^2 g^{-1} to 7.2 m^2 g^{-1} (Table 1). Such low SSA values, typical for perovskites, are mainly a consequence of the high temperature treatment (above 600 °C) which is necessary for formation of the perovskite phase. Development of synthesis methods resulting in reduced particle size, thereby in increased SSA, could allow for the same ORR performance at a lower cathode loading, thus for a smaller cathode layer thickness and for concomitant reduced voltage losses due to mass transport resistances [20]. However, it has to be taken into account that changing particle size can also affect intrinsic ORR activity [38].

The XRD patterns of the six synthesized $La_{0.8}Sr_{0.2}Co_xFe_{1-x}O_{3-\delta}$ oxides (Table 1) are compared in Fig. 1a. They reveal that the perovskite phase is developed and that no secondary phases are formed at detectable levels. The change of the peak located between ca. 32 and 34° (2θ scale) from single (for x = 0 and 0.2) to doublet (for $0.4 \leq x \leq 1$), indicates a change in the unit cell symmetry from orthorhombic to rhombohedral [39,40]. Moreover, the clearly observed gradual shift of the diffraction peaks to higher 2θ values with increasing
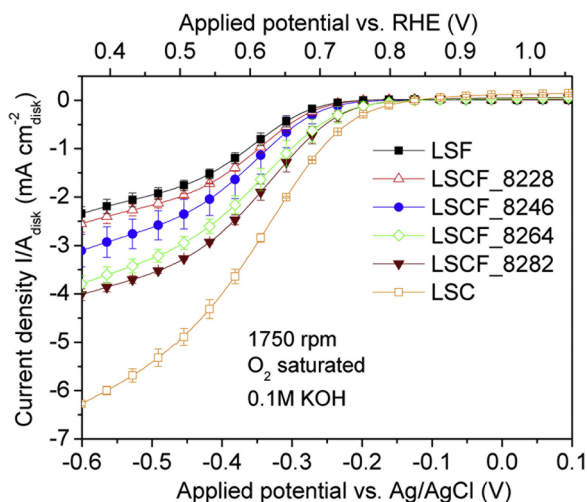
Fig. 2. Polarization curves obtained with the tested $La_{0.8}Sr_{0.2}Co_xFe_{1-x}O_{3-\delta}$/C electrocatalysts (Table 1) in O_2 saturated 0.1 M KOH solution and room temperature; RDE rotation rate: 1750 rpm; Potential scan rate: 5 mV s^{-1} (positive-going scan).

Fig. 3. Onset potential values for the tested $La_{0.8}Sr_{0.2}Co_xFe_{1-x}O_{3-\delta}$/C electrocatalysts (Table 1); O_2 saturated 0.1 M KOH solution and room temperature.

substitution of iron by cobalt (Fig. 1a & b) indicates contraction of the unit cell, which has been mainly attributed to replacement of Fe^{3+} by Co^{3+}, the former having a larger ionic radius than the latter [39–41]. The 2θ shift becomes less pronounced with increasing cobalt content (Fig. 1b), which implies a less pronounced decrease in the size of the unit cell, as observed for $LaCo_xFe_{1-x}O_{3-\delta}$ and attributed to changes in the relative number of Fe^{4+} to Fe^{3+} and Co^{2+} to Co^{3+} accompanying the replacement of Fe^{3+} by Co^{3+} [41].

In Fig. 2 are compared current density (current normalized to the electrode geometric surface area) vs. applied potential curves for the tested electrocatalysts obtained in O_2 saturated 0.1 M KOH solution and at a rotation rate of the RDE equal to 1750 rpm, by linearly varying the electrocatalyst potential in the positive-going direction from -0.6 to 0.1 V vs. Ag/AgCl (0.36 to 1.06 V vs. RHE) at a scan rate of 5 mV s^{-1}. More cathodic potentials were not applied in order to avoid possible irreversible reduction of the perovskites. Each curve in the figure corresponds to the average of the data obtained with at least two different electrocatalysts of the same composition; the standard deviation is shown with error bars at selected potentials. Polarization curves obtained at the other rotation rates are shown in Figs. S1a–S1d (Supplementary material).

As shown in Figs. 2 and S1a-d, over the entire potential range the current density (absolute value) for the same potential decreases with increasing substitution of cobalt by iron in the perovskite composition, which indicates a decreasing apparent ORR activity. However, no conclusions about the intrinsic ORR activity of the electrocatalysts can be drawn without further analysis, as the ORR occurs under conditions of mixed kinetic-mass transfer control over practically the entire range of potentials. It is also noted that the limiting current density region is not reached. As discussed below, the limiting current density was calculated from the slope of the Koutecky – Levich plots.

A quick assessment of the ORR intrinsic activity can be based on the ORR onset potential [5], which was determined by the intersection of the current baseline and the tangent line drawn to the rising part of the polarization curve at the end of the kinetic control region (Fig. S2, Supplementary material). Fig. 3 shows the ORR onset potentials thus determined for the compared electrocatalysts. On the basis of these onset potentials, the ORR activity of the electrocatalysts follows the descending order LSC > LSCF_8282 > LSCF_8264 > LSCF_8246 > LSCF_8228 > LSF, i.e. it decreases with increasing substitution of Co by Fe at the B-sites.

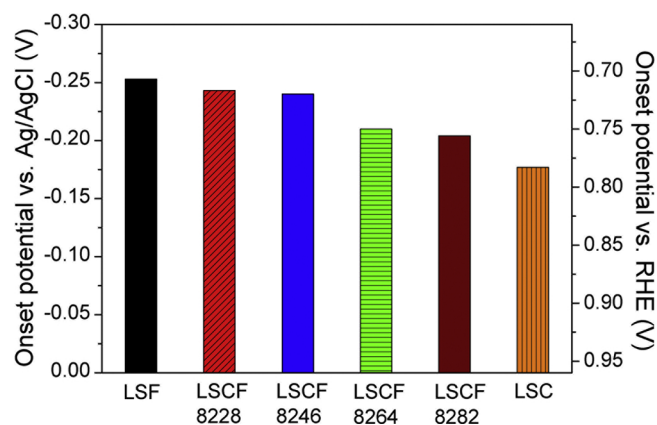In order to compare the intrinsic ORR activities of the perovskite

electrocatalysts, the corresponding kinetic current densities, i_k, i.e. the current densities that would be observed in the absence of mass transport limitations, were determined and compared at the same potential. Kinetic current density for each selected potential and electrocatalyst was calculated from the inverse of the intercept of i^{-1} vs. $N^{-1/2}$ plots (Koutecky – Levich plots), which yield a straight line according to the equation [42]:

$$\frac{1}{i} = \frac{1}{i_k} + \frac{1}{i_{lim}} = \frac{1}{i_k} + \frac{1}{BN^{1/2}} \tag{5}$$

where i is the measured current density, i_k is the kinetic current density, i_{lim} is the limiting current density and N is the RDE rotation rate (in revolutions per min, rpm). The proportionality between i_{lim} and $N^{1/2}$, i.e. the equality $i_{lim} = B \, N^{1/2}$, stems from the Levich equation [42]:

$$i_{lim} = 0.201 \, n \, F \, D^{2/3} \nu^{-1/6} C_b N^{1/2} \tag{6}$$

where F denotes Faraday's constant (C g-eq^{-1}) and ν the kinematic viscosity of the electrolyte (m^2 s^{-1}), whereas, for the ORR, n denotes the number of transferred electrons per reduced O_2 molecule, D the diffusion coefficient (m^2 s^{-1}) of oxygen in the electrolyte solution and C_b the bulk concentration of dissolved oxygen (mol m^{-3}). Levich equation is based on certain assumptions, which are satisfied within a certain range of N values depending on the specific system [42].

Fig. 4a shows Koutecky – Levich plots for the tested electrocatalysts (Table 1) corresponding to applied potential equal to -0.55 V vs. Ag/AgCl (0.41 V vs. RHE) and constructed using the polarization data shown in Fig. 2, for $N = 1750$ rpm, and, in Figs. S1a to S1d (Supplementary material), for the other rotation rates, after correction for the background current (measured in He saturated solution). Straight lines with slopes $B^{-1} = N^{1/2}/i_{lim}$ calculated using Levich equation (Eq. (6)) for electron transfer number $n = 2$ and $n = 4$, respectively, are also shown in the figure, their position being arbitrarily chosen. The following parameter values were used in this calculation, referring to a 0.1 M KOH solution at room temperature [43]: kinematic viscosity $\nu = 10^{-6}$ m^2 s^{-1}, diffusion coefficient of oxygen $D_{O_2} = 1.87 \times 10^{-9}$ m^2 s^{-1} and bulk concentration of oxygen $C_{O_2} = 1.21$ mol m^{-3}. As shown in the figure, the data corresponding to each electrocatalyst fall on a straight line, i.e. Eq. (5) is obeyed, and thus the kinetic current density for the specific potential can be calculated from the inverse of the intercept of this line. Moreover, from the slope of this line and the Levich equation, using the aforementioned parameter values, the number of transferred electrons, n, per reduced oxygen molecule can be calculated. The results of this calculation, for the data presented in Fig. 4a, are shown in Fig. 4b. Visual comparison of the slopes of the straight lines in Fig. 4a, as well as comparison of the n values shown in Fig. 4b, shows that the number of electrons involved in the ORR mechanism changes, almost gradually, with increasing substitution of iron by cobalt at the B-sites,
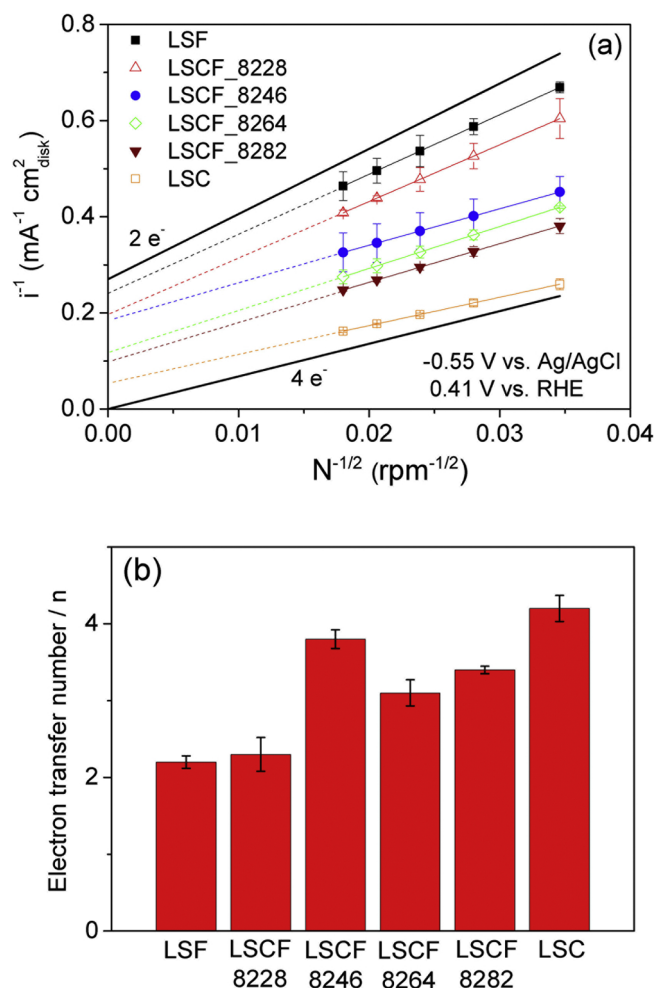
Fig. 5. Mass-transfer corrected Tafel plots for the ORR on the tested $La_{0.8}Sr_{0.2}Co_xFe_{1-x}O_{3-\delta}/C$ electrocatalysts (Table 1), in O_2 saturated 0.1 M KOH solution and room temperature. The kinetic current I_k is normalized to the perovskite oxide surface area, A_{oxide}.

Fig. 4. (a) Koutecky-Levich (K-L) plots for the tested $La_{0.8}Sr_{0.2}Co_xFe_{1-x}O_{3-\delta}/C$ electrocatalysts (Table 1) for applied potential -0.55 V vs. Ag/AgCl (0.41 V vs. RHE); (b) Electron-transfer number n for the ORR, calculated from the slopes of the K-L plots.

Table 2
Average electron transfer number n.

Electrocatalyst	n
LSF/C	2.2 ± 0.08
LSCF_8228/C	2.4 ± 0.24
LSCF_8246/C	3.8 ± 0.13
LSCF_8264/C	3.2 ± 0.18
LSCF_8282/C	3.4 ± 0.05
LSC/C	4.2 ± 0.14

from ca. $2e^-$ for LSF to ca. $4e^-$ for LSC; this indicates a corresponding gradual change in the ORR pathway. The same conclusion concerning the electron transfer number for the tested electrocatalysts was drawn by similar analysis (Koutecky-Levich plots) performed for other potentials in the range -0.4 to -0.6 V vs. Ag/AgCl (0.56 to 0.36 V vs. RHE) (Supplementary material, Figs. S3a to S3f). The calculated average electron transfer number values are listed in Table 2.

The kinetic current values $I_{kin} = i_{kin} A_{disk}$ ($A_{disk} = 0.196$ cm^2) determined from Koutecky-Levich plots for the tested electrocatalysts and different potentials (Figs. 4 & S3a–f) were normalized to the perovskite surface area A_{oxide}, i.e. the product of perovskite mass ($m_{oxide} = 14.5$ μg) and perovskite SSA (Table 1), to calculate the specific activity (S.A.) [34]. In performing this calculation it is assumed that SSA does not differ appreciably from the electrochemically active surface area
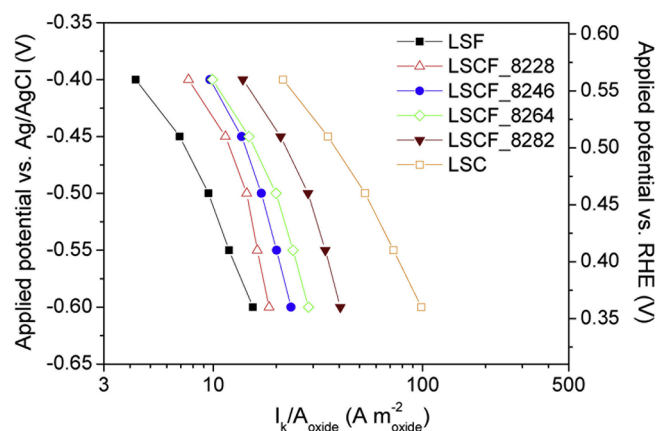
(ECSA), or, at least, that the percentage utilization of SSA in ORR is the same for all compared perovskites. In Fig. 5 is shown in the form of semilogarithmic plots (Tafel plots) the dependence of specific activity on applied potential, for all tested electrocatalysts. It is obvious from the figure that the highest specific activity is exhibited by LSC/C and the lowest by LSF/C, the activity gradually decreasing with increasing substitution of cobalt by iron at the B-sites. This conclusion about the dependence of specific activity on relative occupancy of perovskite B-sites by iron and cobalt is in agreement with that drawn by comparing the onset potentials (Fig. 3). For easier comparison of the activities of the studied electrocatalysts, their specific activity and their mass activity (I_k/perovskite mass) for selected potentials are presented in Fig. 6a and b, respectively, in the form of bar graphs. As shown in Fig. 6a, at all potentials the highest and lowest S.A. were exhibited by LSC/C and LSF/C, respectively, the ratio of their activities increasing from ca. 5.1 to ca. 6.5 with decreasing catalyst potential from -0.4 to -0.6 V vs. Ag/AgCl (0.56 to 0.36 V vs. RHE). As also shown in the figure, at all potentials the specific activity increased with increasing substitution of iron by cobalt at the B-sites. It is noted that comparison of specific activities does not correspond to comparison of turnover frequencies as different number of electrons are exchanged in the ORR on the tested electrocatalysts (Table 2). On the other hand, considering the n values listed in Table 2, it is clear from Fig. 6a that the observed differences in intrinsic activity cannot be merely explained by the corresponding differences in the number of transferred electrons.

Concerning mass activity (M.A.), a similar trend was observed, with slight deviations. As shown in Fig. 6b, at all potentials the highest M.A. was exhibited clearly by LSC/C and the lowest by LSF/C with the exception of -0.6 V vs. Ag/AgCl (0.36 V vs. RHE), at which the lowest M.A was that of LSCF_8228/C, ca. 6% lower than that of LSF/C. The ratio of the mass activities of LSC/C and LSF/C increased from ca. 4.1 to ca. 5.1 with decreasing catalyst potential from -0.4 to -0.6 V vs. Ag/AgCl (0.56 to 0.36 V vs. RHE).

A limited amount of data has appeared in literature concerning the ORR activity of $La_ySr_{1-y}Co_xFe_{1-x}O_3$ in alkaline media, as determined using the thin film RDE technique. Alegre et al. [28] studied both ORR and OER in 1 M KOH on a $La_{0.6}Sr_{0.4}Co_{0.2}Fe_{0.8}O_3$/high surface area carbon black (Ketjenblack) electrocatalyst (perovskite to carbon mass ratio equal to 1:1 and catalyst loading equal to 50 μg cm_{disk}^{-2}). From their Koutecky-Levich plots a value of 3.6 mA cm_{disk}^{-2} for the ORR kinetic current density at 0.5 V vs RHE can be calculated. The kinetic current density value determined in the present work at the same potential for $La_{0.8}Sr_{0.2}Co_{0.2}Fe_{0.8}O_3$/C is higher, equal to 5.0 mA cm_{disk}^{-2}. Nagai et al. [35] measured a current density of ca. 3.6 mA cm_{disk}^{-2} for the ORR on $La_{0.8}Sr_{0.2}Co_{0.6}Fe_{0.4}O_3$ /Vulcan XC-72 at 0.5 V vs RHE (perovskite to
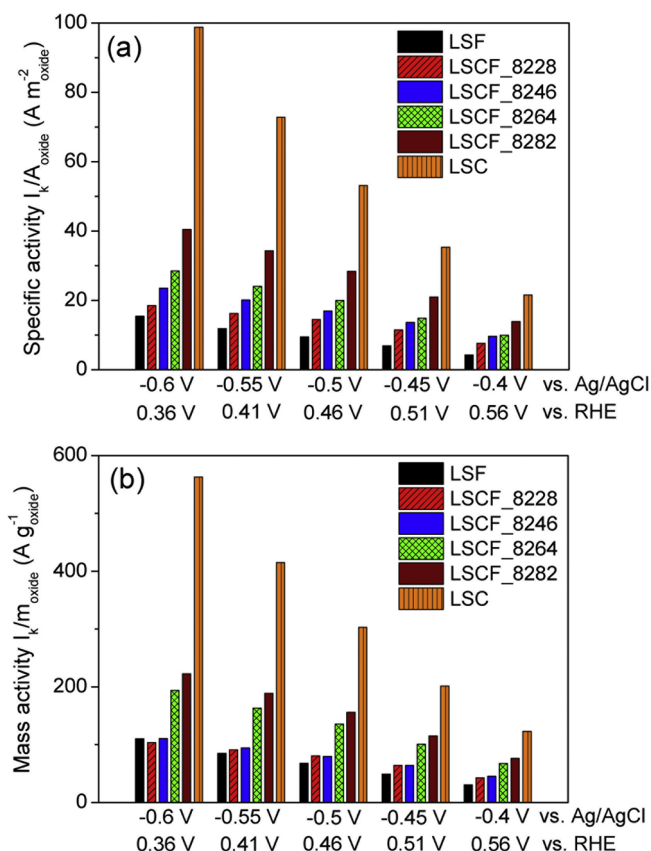
Fig. 6. Bar graphs showing for the tested $La_{0.8}Sr_{0.2}Co_xFe_{1-x}O_{3-\delta}$/C electrocatalysts (Table 1), at selected potentials, the kinetic current I_k normalized (a) to the perovskite oxide surface area, A_{oxide} (specific activity), and (b) to the perovskite mass, m_{oxide}, in the electrode (mass activity).

carbon mass ratio equal to 3:1 and catalyst loading equal to 199 μg cm_{disk}^{-2}, 0.1 M KOH) at 900 rpm. For the same material, but a lower catalyst loading (equal to 98.7 $\mu g\, cm_{disk}^{-2}$) and 830 rpm, a current density of 2.3 $mA\, cm_{disk}^{-2}$ was measured in the present study.

The ORR activity of the most active electrocatalyst tested in the present work (LSC/C) is clearly lower than that of both Pt/C and Pd/C electrocatalysts. ORR onset potentials more positive than 0.93 V vs. RHE have been reported for both 20 wt.% Pt/C and 20 wt.% Pd/C in alkaline medium [5], compared to ca. 0.78 V vs. RHE determined for LSC/C in the present work (Fig. 3). Polarization curves obtained with the LSC/C electrocatalyst, a 10 wt.% Pd/C electrocatalyst prepared via wet impregnation [37] and a commercial 10 wt.% Pt/C electrocatalyst (E-TEK, Lot#2912900) are compared in Fig. S4 (Supplementary material).

The observed in this study gradual increase in the ORR activity of $La_{0.8}Sr_{0.2}Co_xFe_{1-x}O_{3-\delta}$/C (x from 0 to 1) electrocatalysts, in 0.1 M KOH, upon increasing substitution of iron by cobalt at the B-sites can be mainly attributed to concomitant changes in the surface electronic structure of the perovskite [15,17]. As proposed in earlier studies [5,8,44,45], such changes affect the interaction between the oxygen species and the perovskite surface sites in the rate determining step(s), thus affecting ORR activity. Recently, Suntivich et al. [8], in qualitative agreement with the earlier conjecture of Matsumoto et al. [44,45], associated the aforementioned interaction with the transfer to O_2^- (to an O—O orbital) of a localized σ^*-antibonding (e_g) electron of a surface transition metal cation, located in an orbital pointing to the surface anion species. Moreover, they demonstrated that the ORR activity of perovskites is primarily determined by the e_g electron-filling of B-site ions, finding a maximum ORR activity for e_g–filling close to 1, and, secondarily, to the covalency of the B–O bond.

The unit cell symmetry of $La_{0.8}Sr_{0.2}Co_xFe_{1-x}O_3$ perovskites at room temperature has been reported to change from orthorhombic, for x = 0, 0.1 and 0.2, to rhombohedral, for higher x values (0.3 ≤ x ≤ 1) [46]. This change to rhombohedral symmetry was also observed in the present study, for 0.4 ≤ x ≤ 1 (Fig. 1a). For $LaCo_xFe_{1-x}O_3$, such symmetry change from orthorhombic to rhombohedral for x > 0.25 has been associated with a decrease in the e_g electrons of the transition metal cations (B-sites) [41]. As e_g electron-filling of B-site ions is an ORR activity descriptor [8], the aforementioned decrease in the e_g electrons can partly explain the observed increase in ORR activity with increasing substitution of iron by cobalt, taking also into account that e_g electron - filling for similar materials ($LaCoO_3$, $La_{0.5}Ca_{0.5}CoO_{3-\delta}$ and $La_{1-x}Ca_xFeO_3$) is equal or higher than 1, i.e. higher than the e_g-filling approximately corresponding to ORR activity maximum [8]. Besides the unit cell symmetry change, a decrease in e_g electron-filling with increasing substitution of iron by cobalt is also expected based on the contraction of the unit cell volume, reflected in the gradual shift of the XRD peaks to higher 2θ values (Fig. 1). This contraction has been correlated with an increase in the strength of the transition metal – oxygen bond in $LaCo_xFe_{1-x}O_3$ perovskites [39,41], thus with a lowering in the value of e_g electron-filling of B-site ions (equal to 2 for high spin $LaFeO_3$ and 1 for intermediate spin $LaCoO_3$ [8,13,18]) and a stronger interaction with the oxygenated species [47]. It is also noted that the observed in the present study higher ORR activity of $La_{0.8}Sr_{0.2}CoO_3$ compared to that of $La_{0.8}Sr_{0.2}FeO_3$ is in agreement with the higher activity in 0.1 M KOH of $La_{0.5}Ca_{0.5}CoO_3$ compared to $La_{0.5}Ca_{0.5}FeO_3$ shown by Suntivich et al. [8]. Our results are also in agreement with the reported by Sunarso et al. [24] higher ORR activity in 0.1 M KOH of $LaCoO_3$/C compared to that of $LaFeO_3$/C, with both oxides mixed with carbon at a 5:1 mass ratio.

The difference in ORR activity of the tested $La_{0.8}Sr_{0.2}Co_xFe_{1-x}O_{3-\delta}$/C electrocatalysts could also be partly associated with oxygen vacancy formation at the perovskite surface, which may promote oxygen adsorption and charge transfer [17,48]. Several studies have demonstrated the beneficial effect of surface oxygen vacancies on the ORR/OER activity of perovskites [17] as well as on selectivity to 4e⁻ reduction [48], the oxygen vacancies created, for example, via tuning cation deficiency, as in the case of $La_{1-x}FeO_{3-\delta}$ (x ≤ 0.1) [48]. A higher extent of oxygen vacancy formation at the electrode/electrolyte interface during ORR has been correlated with a higher ORR activity in 1 M KOH aqueous solution for two-dimensional $La_{0.8}Sr_{0.2}CoO_3$ model electrodes with different surface orientations [49]. On the basis of results on temperature programmed reduction (TPR) of $La_{0.6}Sr_{0.4}Co_xFe_{1-x}O_{3-\delta}$ [50] and $La_{0.7}Sr_{0.3}Co_{0.80.2}FeO_{3-\delta}$ [51], as well as on the electrochemical redox properties of $La_{0.7}Sr_{0.3}Co_{0.8}Fe_{0.2}O_{3-\delta}$ [51], the redox stability of cobalt ions in $La_{0.8}Sr_{0.2}Co_xFe_{1-x}O_{3-\delta}$ is expected to be lower than that of iron ions. Thus, oxygen vacancy formation at the $La_{0.8}Sr_{0.2}Co_xFe_{1-x}O_{3-\delta}$ surface during electrochemical oxygen reduction is expected to increase with increasing substitution of iron by cobalt, which can result in increased ORR activity and favor 4e⁻ reduction over 2e⁻ reduction [17,48] as observed in the present work. The decrease in oxygen vacancy with increasing substitution of cobalt by iron in $La_{0.6}Sr_{0.4}Co_xFe_{1-x}O_{3-\delta}$ perovkites, reported by García-López et al. [52], can also similarly explain the decrease in ORR activity with increasing iron content observed in our study.

As indicated by earlier studies [5], the ORR on perovskite oxides in alkaline media is complicated and the reaction pathway depends on the intrinsic properties of the perovskite (intrinsic activity, conductivity, surface adsorption properties) and on whether it is mixed with a conducting agent, such as carbon black. Alegre et al. [28] determined an electron transfer number n = 2.3 for the ORR in 1 M KOH solution on $La_{0.6}Sr_{0.4}Co_{0.2}Fe_{0.8}O_3$/C (Ketjenblack), in a 1:1 mass ratio, which indicated a two electrons ORR pathway (Eq. (2)) as predominant, in very good agreement with the present study where an average n = 2.4 was determined for $La_{0.8}Sr_{0.2}Co_{0.2}Fe_{0.8}O_3$/C (Table 2). Mattick et al. [53] used a physics-based generalized electrochemical model to simulate RDE linear sweep voltammetry data obtained

under ORR conditions in 0.1 M KOH using as electrocatalyst $La_{0.6}Sr_{0.4}CoO_{3-\delta}$ mixed with carbon black (Vulcan XC-72) in a 10:1 mass ratio. They concluded that at low cathodic overpotentials (potentials ranging from ca. 0.4 to 0.7 V vs. RHE) reaction (1) occurs in parallel with the sequential combination of reactions (2) and (4), whereas at high cathodic overpotentials (potentials lower than ca. 0.2 V vs. RHE) the $2e^- + 2e^-$ pathway (reactions 2 and 3) becomes dominant. These results can also be considered in agreement with those of the present study, where an average $n = 4.2$ was determined for $La_{0.8}Sr_{0.2}CoO_{3-\delta}/C$ at potentials ranging from ca. 0.35 to 0.55 V vs. RHE, taking into account that the higher percentage of carbon used in this study is expected to favor a pseudo $4e^-$ pathway at comparatively lower overpotentials [5]. The induced improvement in electrical contact between perovskite particles by increasing carbon black to perovskite mass ratio is expected to increase the accessibility of active sites for HO_2^- reduction on the perovskite surface, and, thus, favor a $2e^- + 2e^-$ pathway [5,25]. The extent of HO_2^- reduction increases with increasing activity of the perovskite, which can explain the observed in the present work increase in the determined electron transfer number from ca. 2 for LSF/C, the less active member of the $La_{0.8}Sr_{0.2}Co_xFe_{1-x}O_{3-\delta}/C$ electrocatalysts series, to ca. 4 for LSC/C, the most active member of this series (Table 2). It is noted that the carbon phase of perovskite/carbon composite electrodes has been reported to play an active role in ORR in alkaline media by catalyzing the reduction of oxygen to HO_2^- (Eq. (2)), its catalytic action being coupled with that of the perovskite oxide [5,17,28,34]. This implies that neglecting its contribution may lead to erroneous conclusions when assessing the ORR performance of perovskites in alkaline media [34]. However, in the present study the specific and mass activity of the $La_{0.8}Sr_{0.2}Co_xFe_{1-x}O_{3-\delta}/C$ electrocatalysts was compared at potentials lower than ca. 0.6 V vs RHE (Figs. 5 & 6), for which the relative contribution of carbon black to ORR, as quantified by performing blank experiments (Fig. S5, Supplementary material), was negligible.

4. Conclusions

The oxygen reduction reaction (ORR) in 0.1 M KOH solution and at room temperature was studied for a series of $La_{0.8}Sr_{0.2}Co_xFe_{1-x}O_{3-\delta}/$ carbon black (Vulcan XC-72R) electrocatalysts, via the rotating disk electrode (RDE) technique. The main conclusion was that the ORR activity increased gradually with increasing substitution of iron by cobalt. The highest and lowest activities were exhibited by $La_{0.8}Sr_{0.2}CoO_{3-\delta}/C$ and $La_{0.8}Sr_{0.2}FeO_{3-\delta}/C$, respectively, the ratio of their activities increasing with decreasing catalyst potential from -0.4 to -0.6 V vs. Ag/AgCl (0.56 to 0.36 V vs. RHE), specifically from ca. 5.1 to 6.5 as it concerns specific activity and from ca. 4.1 to ca. 5.1 as it concerns mass activity. The aforementioned increase in activity was accompanied by an increase in the number of transferred electrons, from ca. 2, for $La_{0.8}Sr_{0.2}FeO_{3-\delta}/C$, to ca. 4, for $La_{0.8}Sr_{0.2}CoO_{3-\delta}/C$, which indicates a gradual change in the ORR pathway. The observed differences in ORR activity of the compared perovskites were associated with differences in the surface B-sites electronic structure and in the number of surface oxygen vacancies.

Acknowledgments

Appendix A. Supplementary data

Supplementary material related to this article can be found, in the online version, at doi:https://doi.org/10.1016/j.apcatb.2018.11.015.

References

[1] D. Banham, S. Ye, Current status and future development of catalyst materials and catalyst layers for proton exchange membrane fuel cells: an industrial perspective, ACS Energy Lett. 2 (2017) 629–638, https://doi.org/10.1021/acsenergylett.6b00644.

[2] S. Gottesfeld, D.R. Dekel, M. Page, C. Bae, Y. Yan, P. Zelenay, Y.S. Kim, Anion exchange membrane fuel cells: current status and remaining challenges, J. Power Sources 375 (2018) 170–184, https://doi.org/10.1016/j.jpowsour.2017.08.010.

[3] D.R. Dekel, Review of cell performance in anion exchange membrane fuel cells, J. Power Sources 375 (2018) 158–169, https://doi.org/10.1016/j.jpowsour.2017.07.117.

[4] H.A. Gasteiger, S.S. Kocha, B. Sompalli, F.T. Wagner, Activity benchmarks and requirements for Pt, Pt-alloy, and non-Pt oxygen reduction catalysts for PEMFCs, Appl. Catal. B Environ. 56 (2005) 9–35, https://doi.org/10.1016/j.apcatb.2004.06.021.

[5] X. Ge, A. Sumboja, D. Wuu, T. An, B. Li, F.W.T. Goh, T.S.A. Hor, Y. Zong, Z. Liu, Oxygen reduction in alkaline media: from mechanisms to recent advances of catalysts, ACS Catal. 5 (2015) 4643–4667, https://doi.org/10.1021/acscatal.5b00524.

[6] A.A. Gewirth, J.A. Varnell, A.M. DiAscro, Nonprecious metal catalysts for oxygen reduction in heterogeneous aqueous systems, Chem. Rev. 118 (2018) 2313–2339, https://doi.org/10.1021/acs.chemrev.7b00335.

[7] Z. Chen, D. Higgins, A. Yu, L. Zhang, J. Zhang, A review on non-precious metal electrocatalysts for PEM fuel cells, Energy Environ. Sci. 4 (2011) 3167, https://doi.org/10.1039/c0ee00558d.

[8] J. Suntivich, H.A. Gasteiger, N. Yabuuchi, H. Nakanishi, J.B. Goodenough, Y. Shao-Horn, Design principles for oxygen-reduction activity on perovskite oxide catalysts for fuel cells and metal-air batteries, Nat. Chem. 3 (2011) 546–550, https://doi.org/10.1038/nchem.1069.

[9] A. Brouzgou, S. Song, Z.-X. Liang, P. Tsiakaras, Non-precious electrocatalysts for oxygen reduction reaction in alkaline media: latest achievements on novel carbon materials, Catalysts 6 (2016) 159, , https://doi.org/10.3390/catal6100159.

[10] J. Liu, L. Jiang, B. Zhang, J. Jin, D.S. Su, S. Wang, G. Sun, Controllable synthesis of cobalt monoxide nanoparticles and the size-dependent activity for oxygen reduction reaction, ACS Catal. 4 (2014) 2998–3001, https://doi.org/10.1021/cs500741s.

[11] Q. Zhao, Z. Yan, C. Chen, J. Chen, Spinels: controlled preparation, oxygen reduction/evolution reaction application, and beyond, Chem. Rev. 117 (2017) 10121–10211, https://doi.org/10.1021/acs.chemrev.7b00051.

[12] C. Wei, Z. Feng, G.G. Scherer, J. Barber, Y. Shao-Horn, Z.J. Xu, Cations in octahedral sites: a descriptor for oxygen electrocatalysis on transition-metal spinels, Adv. Mater. 29 (2017) 1606800, , https://doi.org/10.1002/adma.201606800.

[13] W.T. Hong, M. Risch, K.A. Stoerzinger, A. Grimaud, J. Suntivich, Y. Shao-Horn, Toward the rational design of non-precious transition metal oxides for oxygen electrocatalysis, Energy Environ. Sci. 8 (2015) 1404–1427, https://doi.org/10.1039/c4ee03869j.

[14] J.B. Goodenough, B.L. Cushing, Oxide-based ORR catalysts, in: W. Vielstich, H.A. Gasteiger, A. Lamm, H. Yokokawa (Eds.), Handbook of Fuel Cells Fundamentals Technology Applications, John Wiley & Sons, Ltd, 2010, pp. 890–903.

[15] M. Risch, Perovskite electrocatalysts for the oxygen reduction reaction in alkaline media, Catalysts 7 (2017) 154, https://doi.org/10.3390/catal7050154.

[16] L. Zhu, R. Ran, M. Tadé, W. Wang, Z. Shao, Perovskite materials in energy storage and conversion, Asia-Pac. J. Chem. Eng. 11 (2016) 338–369, https://doi.org/10.1002/apj.2000.

[17] Y. Zhu, W. Zhou, Z. Shao, Perovskite/Carbon Composites: Applications in Oxygen Electrocatalysis, Small 13 (2017) 1603793, , https://doi.org/10.1002/smll.201603793.

[18] V. Celorrio, E. Dann, L. Calvillo, D.J. Morgan, S.R. Hall, D.J. Fermin, Oxygen reduction at carbon-supported lanthanides: the role of the B-site, ChemElectrochemChem 3 (2015) 283–291, https://doi.org/10.1002/celc.201500440.

[19] Y. Matsumoto, H. Yoneyama, H. Tamura, A new catalyst for cathodic reduction of oxygen: Lanthanum nickel oxide, Chem. Lett. 4 (1975) 661–662, https://doi.org/10.1246/cl.1975.661.

[20] J. Suntivich, H.A. Gasteiger, N. Yabuuchi, Y. Shao-Horn, Electrocatalytic measurement methodology of oxide catalysts using a thin-film rotating disk electrode, J. Electrochem. Soc. 157 (2010) B1263–B1268, https://doi.org/10.1149/1.3456630.

[21] T. Hyodo, M. Hayashi, N. Miura, N. Yamazoe, Catalytic activities of rare-earth manganites for cathodic reduction of oxygen in alkaline solution, J. Electrochem. Soc. 143 (1996) L266–L267, https://doi.org/10.1149/1.1837229.

[22] K.A. Stoerzinger, W. Lü, C. Li, T. Ariando, Y. Venkatesan, Y. Shao-Horn, Highly active epitaxial $La_{(1-x)}Sr_xMnO_3$ surfaces for the oxygen reduction reaction: role of charge transfer, J. Phys. Chem. Lett. 6 (2015) 1435–1440, https://doi.org/10.1021/acs.jpclett.5b00439.

[23] Y. Xue, H. Miao, S. Sun, Q. Wang, S. Li, Z. Liu, $(La_{1-x}Sr_x)_{0.98}MnO_3$ perovskite with A-site deficiencies toward oxygen reduction reaction in aluminum-air batteries, J. Power Sources 342 (2017) 192–201, https://doi.org/10.1016/j.jpowsour.2016.12.065.

[24] J. Sunarso, A.A.J. Torriero, W. Zhou, P.C. Howlett, M. Forsyth, Oxygen reduction reaction activity of La-based perovskite oxides in alkaline medium: a thin-film

rotating ring-disk electrode study, J. Phys. Chem. C 116 (2012) 5827–5834, https://doi.org/10.1021/jp211946n.

[25] T. Poux, A. Bonnefont, G. Kerangueven, G.A. Tsirlina, E.R. Savinova, Electrocatalytic oxygen reduction reaction on perovskite oxides: series versus direct pathway, ChemPhysChem 15 (2014) 2108–2120, https://doi.org/10.1002/cphc.201402022.

[26] C. Jin, X. Cao, F. Lu, Z. Yang, R. Yang, Electrochemical study of $Ba_{0.5}Sr_{0.5}Co_{0.8}Fe_{0.2}O_3$ perovskite as bifunctional catalyst in alkaline media, Int. J. Hydrogen Energy 38 (2013) 10389–10393, https://doi.org/10.1016/j.ijhydene.2013.06.047.

[27] J. Suntivich, K.J. May, H.A. Gasteiger, J.B. Goodenough, Y. Shao-Horn, A perovskite oxide optimized for oxygen evolution catalysis from molecular orbital principles, Science 334 (2011) 1383–1385, https://doi.org/10.1126/science.1212858.

[28] C. Alegre, E. Modica, A.S. Aricò, V. Baglio, Bifunctional oxygen electrode based on a perovskite/carbon composite for electrochemical devices, J. Electroanal. Chem. 808 (2018) 412–419, https://doi.org/10.1016/j.jelechem.2017.06.023.

[29] D.A. Fumo, J.R. Jurado, A.M. Segadaes, J.R. Frade, Combustion synthesis of iron-substituted strontium titanate perovskites, Mater. Res. Bull. 32 (1997) 1459–1470, https://doi.org/10.1016/S0025-5408(97)00117-7.

[30] A. Civera, M. Pavese, G. Saracco, V. Specchia, Combustion synthesis of perovskite-type catalysts for natural gas combustion, Catal. Today 83 (2003) 199–211, https://doi.org/10.1016/s0920-5861(03)00220-7.

[31] L. da Conceição, A.M. Silva, N.F.P. Ribeiro, M.M.V.M. Souza, Combustion synthesis of $La_{0.7}Sr_{0.3}Co_{0.5}Fe_{0.5}O_3$ (LSCF) porous materials for application as cathode in IT-SOFC, Mater. Res. Bull. 46 (2011) 308–314, https://doi.org/10.1016/j.materresbull.2010.10.009.

[32] J. Niu, J. Deng, W. Liu, L. Zhang, G. Wang, H. Dai, H. He, X. Zi, Nanosized perovskite-type oxides $La_{1-x}Sr_xMO_{3-\delta}$ (M = Co, Mn; x = 0, 0.4) for the catalytic removal of ethylacetate, Catal. Today 126 (2007) 420–429, https://doi.org/10.1016/j.cattod.2007.06.027.

[33] A.E. Danks, S.R. Hall, Z. Schnepp, The evolution of 'sol–gel' chemistry as a technique for materials synthesis, Mater. Horiz. 3 (2016) 91–112, https://doi.org/10.1039/c5mh00260e.

[34] T. Poux, F.S. Napolskiy, T. Dintzer, G. Kéranguéven, S.Y. Istomin, G.A. Tsirlina, E.V. Antipov, E.R. Savinova, Dual role of carbon in the catalytic layers of perovskite/carbon composites for the electrocatalytic oxygen reduction reaction, Catal. Today 189 (2012) 83–92, https://doi.org/10.1016/j.cattod.2012.04.046.

[35] T. Nagai, S.-i. Yamazaki, M. Asahi, Z. Siroma, N. Fujiwara, T. Ioroi, Metalloporphyrin-modified perovskite-type oxide for the electroreduction of oxygen, J. Power Sources 293 (2015) 760–766, https://doi.org/10.1016/j.jpowsour.2015.06.004.

[36] K.J.J. Mayrhofer, D. Strmcnik, B.B. Blizanac, V. Stamenkovic, M. Arenz, N.M. Markovic, Measurement of oxygen reduction activities via the rotating disc electrode method: from Pt model surfaces to carbon-supported high surface area catalysts, Electrochim. Acta 53 (2008) 3181–3188, https://doi.org/10.1016/j.electacta.2007.11.057.

[37] G. Bampos, S. Bebelis, D.I. Kondarides, X. Verykios, Comparison of the activity of Pd–M (M: Ag, Co, Cu, Fe, Ni, Zn) bimetallic electrocatalysts for oxygen reduction reaction, Top. Catal. 60 (2017) 1260–1273, https://doi.org/10.1007/s11244-017-0795-z.

[38] M. Retuerto, A.G. Pereira, F.J. Pérez-Alonso, M.A. Peña, J.L.G. Fierro, J.A. Alonso, M.T. Fernández-Díaz, L. Pascual, S. Rojas, Structural effects of $LaNiO_3$ as electrocatalyst for the oxygen reduction reaction, Appl. Catal. B Environ. 203 (2017) 363–371, https://doi.org/10.1016/j.apcatb.2016.10.016.

[39] N.A. Merino, B.P. Barbero, P. Ruiz, L.E. Cadús, Synthesis, characterisation, catalytic activity and structural stability of $LaCo_{1-y}Fe_yO_{3\pm\lambda}$ perovskite catalysts for combustion of ethanol and propane, J. Catal. 240 (2006) 245–257, https://doi.org/10.1016/j.jcat.2006.03.020.

[40] M.M. Natile, F. Poletto, A. Galenda, A. Glisenti, T. Montini, L. De Rogatis, P. Fornasiero, $La_{0.6}Sr_{0.4}Co_{1-y}Fe_yO_{3-\delta}$ perovskites: influence of the Co/Fe atomic ratio on properties and catalytic activity toward alcohol steam-reforming, Chem. Mater. 20 (2008) 2314–2327, https://doi.org/10.1021/cm703329k.

[41] A. Gholizadeh, The effects of A/B-site substitution on structural, redox and catalytic properties of lanthanum ferrite nanoparticles, J. Mater. Res. Technol. (2018), https://doi.org/10.1016/j.jmrt.2017.12.006 xxx, in press.

[42] E. Gileadi, Electrode Kinetics for Chemists, Chemical Engineers and Materials Scientists, VCH Publishers, Inc., New York, 1993.

[43] H.S. Kushwaha, A. Halder, P. Thomas, R. Vaish, $CaCu_3Ti_4O_{12}$: a bifunctional perovskite electrocatalyst for oxygen evolution and reduction reaction in alkaline medium, Top. Catal. 252 (2017) 532–540, https://doi.org/10.1016/j.electacta.2017.09.030.

[44] Y. Matsumoto, H. Yoneyama, H. Tamura, Influence of the nature of the conduction band of transition metal oxides on catalytic activity for oxygen reduction, J. Electroanal. Chem. 83 (1977) 237–243, https://doi.org/10.1016/S0022-0728(77)80169-1.

[45] Y. Matsumoto, H. Yoneyama, H. Tamura, Catalytic activity for electrochemical reduction of oxygen of lanthanum nickel-oxide and related oxides, J. Electroanal. Chem. 79 (1977) 319–326, https://doi.org/10.1016/S0022-0728(77)80453-1.

[46] L.-W. Tai, M.M. Nasrallah, H.U. Anderson, D.M. Sparlin, S.R. Sehlin, Structure and electrical properties of $La_{1-x}Sr_xCo_{1-y}Fe_yO_3$. Part 1. The system $La_{0.8}Sr_{0.2}Co_{1-y}Fe_yO_3$, Solid State Ion. 76 (1995) 259–271, https://doi.org/10.1016/0167-2738(94)00245-N.

[47] H. Zhu, P. Zhang, S. Dai, Recent Advances of Lanthanum-Based Perovskite Oxides for Catalysis, ACS Catal. 5 (2015) 6370–6385, https://doi.org/10.1021/acscatal.5b01667.

[48] Y. Zhu, W. Zhou, J. Yu, Y. Chen, M. Liu, Z. Shao, Enhancing electrocatalytic activity of perovskite oxides by tuning cation deficiency for oxygen reduction and evolution reactions, Chem. Mater. 28 (2016) 1691–1697, https://doi.org/10.1021/acs.chemmater.5b04457.

[49] M. Komo, A. Hagiwara, S. Taminato, M. Hirayama, R. Kanno, Oxygen evolution and reduction reactions on $La_{0.8}Sr_{0.2}CoO_3$ (001), (110), and (111) surfaces in an alkaline solution, Electrochemistry 80 (2012) 834–838, https://doi.org/10.5796/electrochemistry.80.834.

[50] J.N. Kuhn, U.S. Ozkan, Effect of Co Content Upon the Bulk Structure of Sr- and Co-doped $LaFeO_3$, Catal. Lett. 121 (2007) 179–188, https://doi.org/10.1007/s10562-007-9364-6.

[51] E. Siebert, C. Roux, A. Boréave, F. Gaillard, P. Vernoux, Oxido-reduction properties of $La_{0.7}Sr_{0.3}Co_{0.8}Fe_{0.2}O_{3-\delta}$ perovskite oxide catalyst, Solid State Ionics 183 (2011) 40–47, https://doi.org/10.1016/j.ssi.2010.11.012.

[52] E. García-López, G. Marcì, F. Puleo, V. La Parola, L.F. Liotta, $La_{1-x}Sr_xCo_{1-y}Fe_yO_{3-\delta}$ perovskites: Preparation, characterization and solar photocatalytic activity, Appl. Catal. B Environ. 178 (2015) 218–225, https://doi.org/10.1016/j.apcatb.2014.09.014.

[53] V.F. Mattick, X. Jin, T. Yang, R.E. White, K. Huang, Unraveling Oxygen Electrocatalysis Mechanisms on a Thin-Film Oxygen-Deficient Perovskite $La_{0.6}Sr_{0.4}CoO_{3-\delta}$, ACS Appl. Energy Mater 1 (2018) 3937–3946, https://doi.org/10.1021/acsaem.8b00669 xxx, in press.